Available online at www.sciencedirect.com
SCIENCE DIRECT®
Atmospheric Environment 39 (2005) 739–747
ATMOSPHERIC ENVIRONMENT
www.elsevier.com/locate/atmosenv

A case study of the size-resolved individual particles collected at a ground-based site on the west coast of Japan during an Asian dust storm event

Chang-Jin Ma*, Susumu Tohno, Mikio Kasahara

Department of Socio-Environmental Energy Science, Graduate School of Energy Science, Kyoto University, Uji, Kyoto 611-0011, Japan

Received 17 March 2004; received in revised form 22 September 2004; accepted 29 September 2004

Abstract

To investigate the nature of individual Asian dust storm particles, an intensive field measurement was carried out on the west coast of Japan during a dense Asian dust storm event in March 2002. The giant particles ($>5\,\mu m$) marked 124 times higher number concentration in the Asian dust storm event than in a non-Asian dust storm period. For the quantification analysis of the ultratrace elements in the size-resolved individual particles, an X-ray microprobe system equipped with super photon ring-8 GeV (SPring-8) BL-39XU was employed. By using this SPring-8 system we could successfully carry out the reconstruction of elemental maps and the quantification analysis of multiple elements in individual particles. The mass of Si showing the maximum value in individual particles was varied in the range from 1.2×10^{-2} pg to 1.1×10^{0} pg with median 1.4×10^{-1} pg. In the case of S, mass ranged from 1.6×10^{-2} pg to 6.7×10^{-2} pg with median 3.9×10^{-2} pg, while several minor trace elements like V, Cr, Cu, and Zn show relatively low masses. A strong particle-size dependency of elemental masses was found for all elements, in particular the elemental masses of soil-derived components showed the monomodal maximum values around 2.05–5.07 μm particle size. From the X-ray, fluorescence images replayed corresponding to individual particles, we could simply categorize the visualized particles into two groups, namely internally mixed particles and externally mixed particles. From the factor analysis with variables of each elemental mass in individual particles, 79% of total particle population was found to be modified by sea-salt and sulfur.

Keywords: Asian dust storm; Individual particles; X-ray microprobe system; Elemental mass; Modification

1. Introduction

Springtime weather in Asia causes intense windstorm events that can pass over the Gobi Desert along the northern China/Mongolia border and other desert regions in China. These winds are capable of generating the huge yellow clouds of suspended dust that are based on the direction of the prevailing wind can be sent out to sea (Kim et al., 2003). Sometimes these dust storms are so immense that they can complete a 5–7-day journey across the Korean Peninsula, Japan Island, and Pacific Ocean. The dust clouds finally dissipate when the particles are removed from the atmosphere by dry and wet removal processes. Gravitational settling of giant particles larger than 10 μm occurs near the source within the first day of transport. Wet removal occurs

*Corresponding author. Tel.: +81 774 38 4413; fax: +81 774 38 4411.
E-mail address: ma@uji.energy.kyoto-u.ac.jp (C.-J. Ma).

1352-2310/$ - see front matter © 2004 Elsevier Ltd. All rights reserved.
doi:10.1016/j.atmosenv.2004.09.073

sporadically throughout the 5–10-day lifetime of the remaining smaller size dust particles. A large number of studies on Asian dust storms have been reported (Duce et al., 1980; Braaten and Cahill, 1986; Nishikawa and Kanamori, 1991; Wang and Guanghua, 1996; Zhang et al., 2001; Chun et al., 2001). However, the chemical analyses of Asian dust storm (ADS) particles were usually conducted by collecting many particles on a filter or impactor stage, followed by bulk-sample analysis to deduce particle composition. Unfortunately, these methods obscure the particle-to-particle composition variations. Since a long sampling duration time is required for particle analysis using commercially available aerosol instrumentation, the particle composition may be altered during the collection process due to condensation or evaporation of volatile compounds or chemical reactions. From this point of view, one of the main advantages of single particle analysis is that it is not necessary to sample for a long time. Also, the investigation of the properties of single particles is an essential prerequisite for understanding chemical reactions in the atmosphere (Hinz et al., 1998). Moreover, in some cases, the single-particle analysis data can be used for "finger printing" diverse aerosols, natural as well as anthropogenic. Iwasaka et al. (1988) suggested the importance of a weak ADS event from the thin-film method as an identification method for single particles. Zhang and Iwasaka (1998) reported the morphological and chemical composition of ADS particles using the SEM-EDX technique. However, only a few studies on the quantitative chemical analysis for individual ADS particles, which can provide detailed information about the nature and composition of single dust particles, were reported.

In this study, for the purpose of investigating the nature of size-resolved individual ADS particles, an intensive field measurement was carried out on the west coast of Japan during a dense ADS event in March 2002. An X-ray microprobe system equipped at SPring-8, BL-39XU was applied for the quantification analysis of the ultra trace elements in the individual ADS particles. This SPring-8 is the world's largest third-generation synchrotron radiation facility and provides the most powerful synchrotron radiation for the analysis of infinitesimal trace elements from various samples including individual airborne particles. In this study, we report the physicochemical nature of size-resolved individual ADS particles collected at a ground-based site on the west coast of Japan.

2. Experimental

2.1. Sampling

Aerosol sampling was performed at a ground-based site on the west coast of Japan during a dense ADS event in March 2002. Our ground-based sampling station is located at Yasaka (35.37°N, 135.81°E) in the north part of Kyoto Prefecture, Japan. This northern part of Kyoto Prefecture is characterized by textile handicraft manufacturing and fishery. About 70% of the total land area is covered by highlands and other mountainous features. Northern Kyoto Prefecture has a typical marine climate, with heavy rains and heavy snow from the effects of seasonal winds. The location of our sampling site is indicated by a filled circle in Fig. 1. Due to the size dependence of the chemical composition of particles, the sampling of size-segregated aerosol particles is required. For the sampling of aerosols as a function of their size, a low pressure Andersen impactor (LPAI) was employed. Aerosol particles were collected onto the 25 mm non-hole polycarbonate filter (Nuclepore). Aerosol particles were classified into five-size steps, i.e. the first stage with 7.65 μm cutoff diameter, the second with 5.07 μm cutoff diameter, the third with 3.45 μm cutoff diameter, the fourth with 2.05 μm cutoff diameter, and the fifth with 1.17 μm cutoff diameter. Since the particles are collected by forming a spot on each stage of LPAI, a long sampling duration time is not desirable for single particle analysis. Therefore, we adjusted the sampling time from 45 to 90 min depending

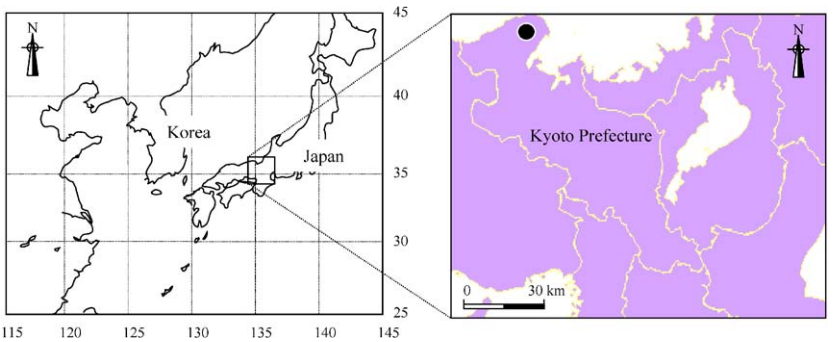

Fig. 1. Map showing sampling location. Field measurement was carried out at Yasaka (35.37°N; 135.81°E), Tango peninsular in Japan.

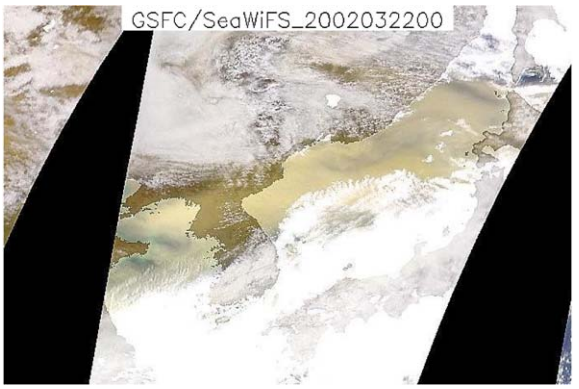

Plate I. The SeaWiFS images on East Asia area on 22 March 2002.

on LPAI stage. Also, the number-size distribution of aerosol particles was measured using an optical particle counter (OPC) (RION, KC-01D) during both ADS and non-Asian dust storm (NADS) periods. The OPC was operated every 15 min in the dynamic range of $>0.3\,\mu m$ with five-step cutoff diameter of 0.3–0.5, 0.5–1.0, 1.0–2.0, 2.0–5.0, and $>5\,\mu m$. The flow rate for the OPC was $3\times10^{-2}\,m^3\,h^{-1}$. The accuracy of the OPC's sizing was checked by the manufacturer (RION). Four-step known size monodisperse polystyrene type latex (PSL) spheres (0.294, 0.505, 1.001 and 2.106 μm) were employed. The PSL particle sizes are traceable to National Institute of Standards and Technology USA (NIST). The PSL was mixed with filtered air in the mixing chamber. Though the shapes of ambient particles, especially those of dust particles, are quite different from the PSL spheres, the OPC sizing accuracy check was conducted by sampling of PSL particles. During the sampling period, the range of wind speed was $2.4–3.5\,m\,s^{-1}$. The ranges of temperature and relative humidity were 7.7–15.6 °C and 47–65%, respectively. Plate I displays the SeaWiFS images provided by NASA (http://seawifs.gsfc.nasa.gov/cgibrs/seawifs) of the East Asia area on 22 March 2002. This shows the development of a large dust storm above the Chinese continent, Korean Peninsula, and Japan Island and its movement to the east. In our sampling period, the longitudinal mixing between air masses in accordance with the arrangement of high- and low-pressure systems could be expected.

2.2. Chemical analysis of individual particles

The X-ray microprobe system equipped at SPring-8, BL-39XU was applied to the quantification analysis of ultratrace elements in the size-solved individual ADS particles ($>1.17\,\mu m$). This method can be successfully used to carry out the reconstruction of elemental maps and for the quantification analysis for multiple elements with fg level sensitivity (Ma et al., 2004). To make the narrow X-ray beam with a microscale, a pair of elliptical mirrors (Kirkpatrick and Baez mirror, KB mirror) was installed to the optical path. A combination of the focusing mirror and a fixed exit monochromator enabled an energy tunable X-ray microbeam. A sample was placed on the XY stage in a vacuum chamber, and a takeoff angle of 10° was used for the measurement. The intensity of the incident X-rays was monitored by an ionization chamber. The fluorescence X-rays were recorded with an Si(Li) detector placed in the electron orbit plane of the storage ring and mounted at 90° to the incident X-rays to minimize background inference caused by the scattering. A sample-detector distance of 100 mm was used to avoid excessive counting rate. The XRF spectra of particles and the substrate film were measured with the data acquisition time of 200 s to realize elemental quantification. The incident beam intensity was evaluated from the Ar XRF signal. The areal density of multiple elements were calculated from the comparisons of the gross signals between the sample and the reference threefold (Cr, Fe, Ni) thin films, and the amount of the elements in individual particles were calculated from the beam size. Details of the calibration of the X-ray microprobe system to yield quantitative measures of elemental mass in individual particles including the effects of the self-absorption are described elsewhere (Hayakawa et al., 2001).

3. Results and discussion

In order to track a wind parcel during our sampling period, a trajectory model, which is primarily used as a diagnostic tool to evaluate the flow field of the atmosphere, was applied. The result of backward trajectory analysis is shown in Fig. 2 represents the flow from a single point (35.37°N, 135.81°E) started at the initial time (00 UTC, 22 March 2002). The Gobi desert area is also illustrated in Fig. 2. This trajectory result was produced using the NOAA ARL Website (www.arl.noaa.gov/ready/). Three kinds of trajectory pathways (from 1000, 2000, and 3000 m above model ground level (AGL)) were measured. This NOAA's hybrid single-particle Lagrangian integrated trajectory (HYSPLIT) trajectory map shows an aerial view of the paths of an air parcel and a vertical view of its movement at three different altitudes. The circles, squares, and triangles lying on each line indicate the position of the air parcel over 48 h. This backward-trajectory analysis indicates that the prevailing winds at the three altitudes in our sampling period originated in desert areas of China and the air parcel arrived at our sampling site in 48 h.

Fig. 3 shows the time-series variation of particle number concentration at ground-based site on the west coast of Japan during an ADS on 22 March 2002 and a

NADS on 30 May 2002. The number-size distribution of particles larger than 1 μm was used for the comparison between ADS and NADS periods. For small particles in the range of 1.0–2.0 μm the particle number concentration was slightly increased during an ADS compared with that in a NADS period. However, the particles between 2 and 5 μm show a remarkable increase during an ADS event. In particular, the giant particles (larger than 5 μm) marked 124 times higher concentration in an ADS event than in a NADS period. This high number concentration of large particles was distinctly shown especially around midday. Though these results are limited in case level, the particle number concentration obtained in our case study is in good agreement with that of early measurement by Chun et al. (2001).

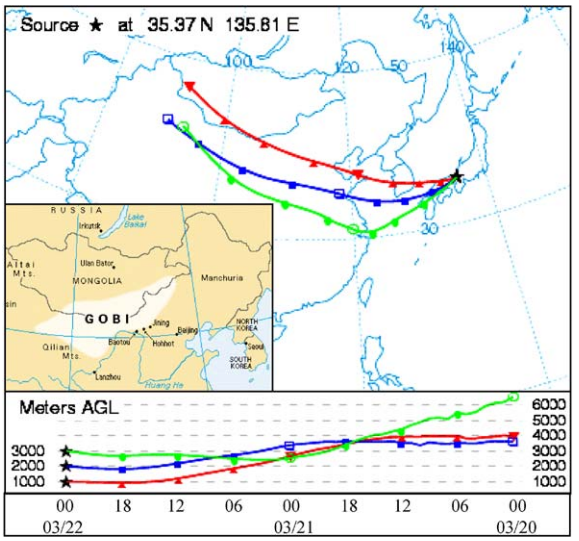

Fig. 2. Backward trajectory started at 35.37°N; 135.81°E. Starting time was at 00 UTC, 22 March 2002. The vertical view at the bottom of the map shows the height of the air parcel measured at corresponding thick marks. The height of the air parcel was measured in hector pascals (HPA). The map of Gobi desert area is also drawn.

The Fe XRF maps for the individual coarse and fine particles are shown at the top in Fig. 4. Coarse and fine particles refer to the particles collected on the second-stage (5.07 μm cutoff diameter) and the fifth-stage (1.17 μm cutoff diameter) of LPAI. In Fig. 4, the separated elemental maps for individual particles are well drawn in the scanning area of around 100 μm × 100 μm. However, the size of elemental map for a single particle does not agree with that of LPAI's cut off because the XRF elemental map can be roughly drawn by the pixels with around several micrometers. The XRF spectra for two coarse and fine particles are plotted at the bottom in Fig. 4. The coarse particles shown by bold solid and bold dotted lines in the spectra show a higher XRF count than the fine particles illustrated by fine solid and fine dotted lines for soil-originated components like Al, Si, K, Ca, Ti, and Fe. On the other hand, although crustal components coexist, several minor trace elements like Ni, Cu, and Zn show a high XRF count in the fine particles.

The summary of elemental masses for ten major elements in individual particles calculated from X-ray microprobe system equipped at SPring-8 BL-39XL are illustrated by the box plot in Fig. 5. Total number of particles from the first to the fifth stage of LPAI is 470. In Fig. 5, max. and min. are the largest and the smallest values in the mass distribution of each element. Med. is

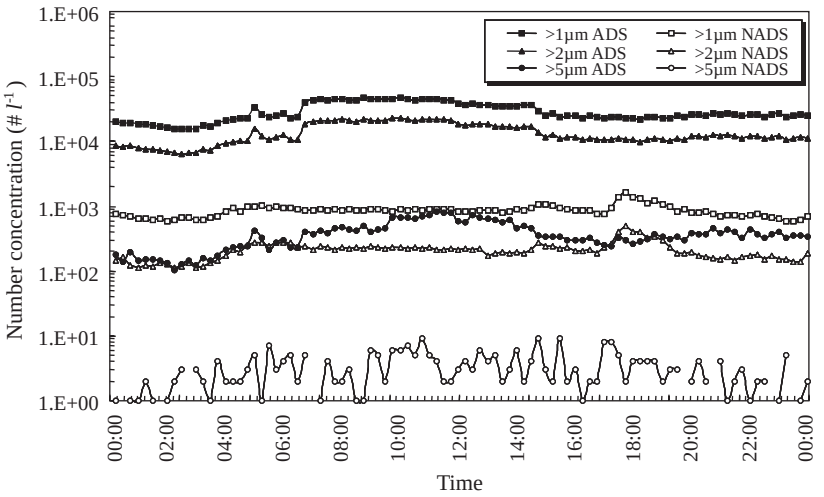

Fig. 3. Time series variation of particle number concentration in Tango Peninsular during ADS, 22 March 2002 and NADS, 30 May 2002 periods.

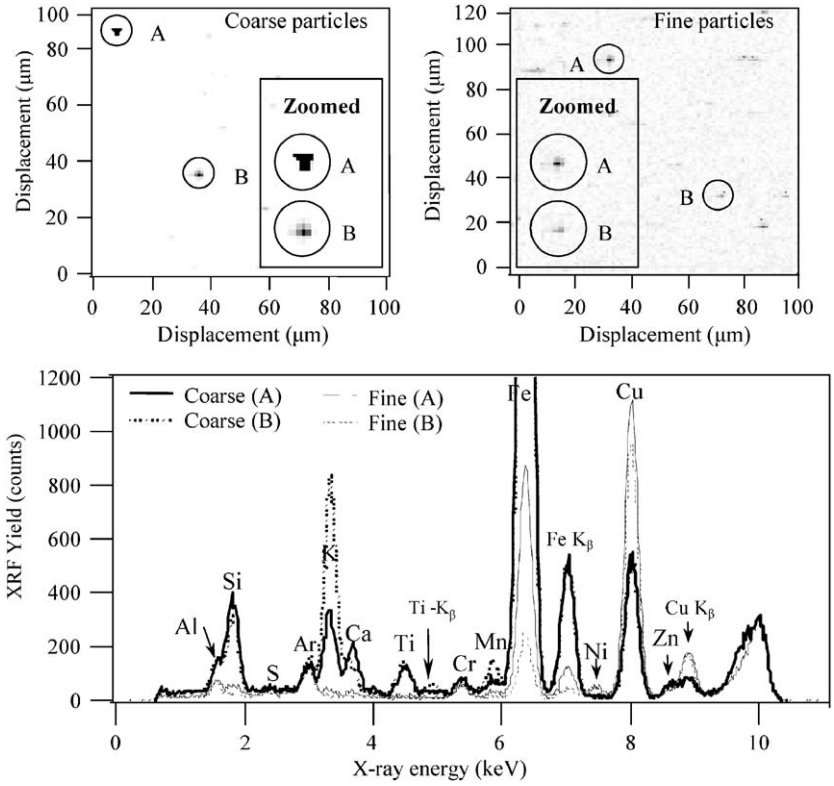

Fig. 4. The XRF elemental maps of individual coarse particles (top left) and fine particles (top right) and their XRF spectra (bottom). The sizes of coarse and fine particles are 5.07 and 1.17 μm, respectively.

a measure of the center that is the middle value in the elemental mass distribution. This median splits the data into two parts, i.e. the upper portion and the lower portion. The upper quartile is the median of the upper half of the data and the lower quartile is the median of the lower half of the data. As might be expected, the soil originated components like Si, Ca, and Fe show relatively high mass levels compared with other elements. As one of the representative soil components, the mass of Si in individual particles varied in the range from 1.2×10^{-2} pg to 1.1×10^{0} pg with median 1.4×10^{-1} pg. In the case of S, mass varied from 1.6×10^{-2} pg to 6.7×10^{-2} pg with median 3.9×10^{-2} pg, while several minor trace elements like V, Cr, Cu, and Zn show a low mass. For nearly all elements, the distribution of the mass set is skewed toward low values with severe scatter. The elements showing severe scattering, except K, Cr, and Cu, indicate that the individual particles collected during our intensive measurement have a complex chemical nature derived from various mechanisms. A comprehensive detailed discussion will be mentioned in the latter half of this manuscript concerning the sources interpretation for individual particles. The size distribution of average elemental mass for individual particles is shown in Fig. 6. A strong particle-size dependency of elemental masses was found for all elements in individual particles. In the case of soil derived components such as Al, Si, P, Fe, and Ca, elemental masses vary as a function of particle size showing the monomodal maximum values at 2.05–5.07 μm particle size. Also, there was a tendency to steeply increase in masses at 2.05 μm particle size. However, the masses of S and Cl are distributed as bimodal distributions with the major peak at giant particles larger than 7.65 μm. Detailed information, like the air parcel movement in inland China and elemental individual composition of desert soil, is needed to explain S distributed in coarse fraction. It seems to indicate that S coexists with the large Asian dust particles as the chemical mixing state. Also, as compared with the masses of soil originated components, the minor elements like Sc, V, Mn, and Ni have negligible masses, and their particle size-distribution was found to be monomodal distribution with the maximum value at 2.05–3.45 μm particle size.

As mentioned earlier, the Asian dust particles can be also modified by sea-salts. This modification most probably occurs by the collisions and coagulations of dust particles and sea-salt particles. The XRF elemental maps for large particles were compared to investigate the transformation of dust particles by sea-salts. Fig. 7

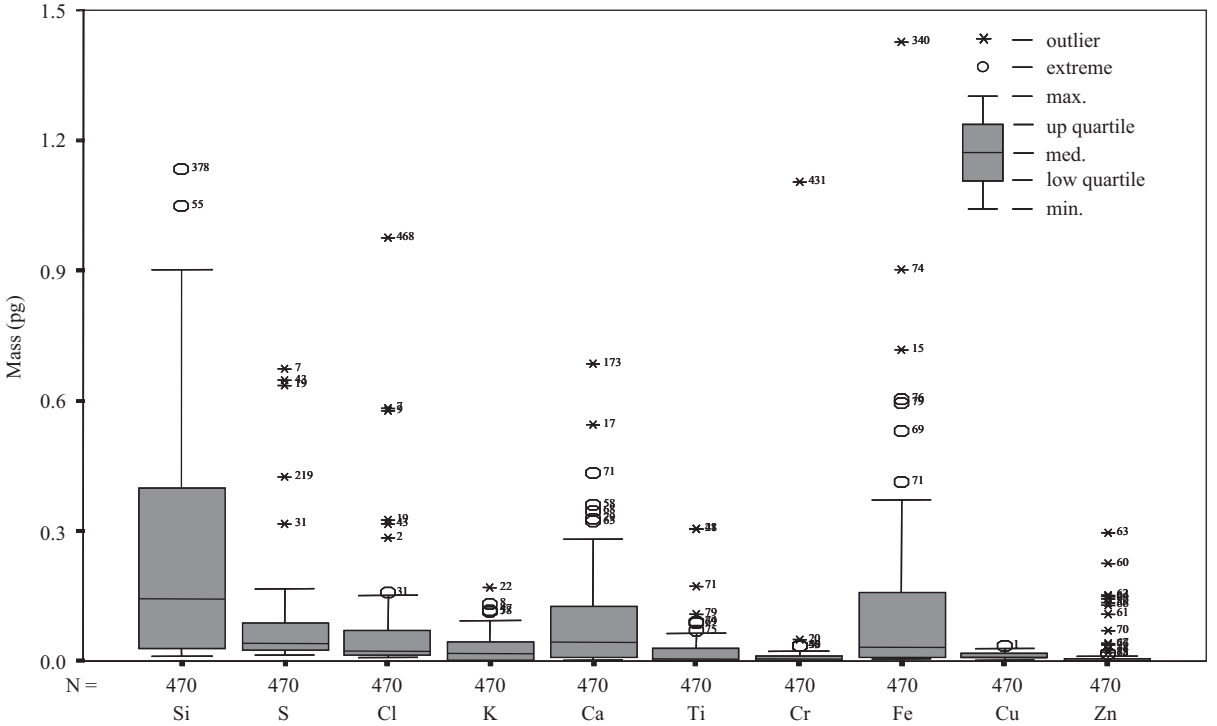

Fig. 5. Box plots of each elemental mass calculated from X-ray microprobe system equipped at SPring-8, BL-39XU. Total particle number is 470.

shows the XRF images of Ca, Si, Cl, and Zn in individual coarse particles collected on the first stage of LPAI (5.07 μm cutoff diameter). These visualized elemental maps enable us not only to presume the chemical mixing state of individual particles, but also to estimate their source profiles. In Fig. 7, the particles enclosed with squares indicate the chemical mixing state with soil originated components and Cl, whereas the particles surrounded by circles show the chemically mixed particles with crustal, marine, and zinc. In addition, several particles indicated by an arrow in Fig. 7 exist independently on each XRF image. From these four kinds of XRF images replayed corresponding to individual particles, we can simply fractionate the visualized particle images into two groups, namely internally mixed particles (particles contain a uniform mixture of components from each of the sources) and externally mixed particles (each particle arises from only one source). As in a typical example of internally mixed particles, the particles enclosed with squares and circles are present at the same displacement portion in the XRF image.

For the purpose of classifying the individual coarse (3.45–5.07 μm) particles, as one of the statistical techniques, factor analysis with variables of each elemental mass in individual particles was applied. Factor analysis was performed on 89 variables (number of particles) and 10 cases (number of elements). The matrix of interelemental correlation was constructed as shown in Fig. 8. The squared multiple correlations obtained from the inverted matrix of inter-correlations were used as the initial communality estimates. The procedures of factor analysis chosen in this study are as follows: choosing the variable and case (numbers of variable and case)—choosing the factoring method (extraction method and number of factor)—making the matrix of correlation coefficient—factor rotating (Varimax with Kaiser normalization)—determining the quality of the result—calculation of factor score. Fig. 9 shows the components plot in rotated space. This three-dimensional scatterplot is a visualization technique for combining factor space and variable space. In Fig. 9 the factor space, defined by component 1, component 2, and component 3, was determined from the interelemental correlation in Fig. 8. In this rotated space, particles can be categorized into three groups, namely group 1, group 2, and group 3, respectively. Group 1 with 21% of total particle population located in the top cluster was found to be high loading in factor containing absolutely high mass for soil components. Group 2 with 52% of total particle population formed in the middle cluster is showing soil and sulfur (from coal burning and other sources)-rich. Group 3 with poor clustering has high loading in factor with coexisting of crustal, marine, and

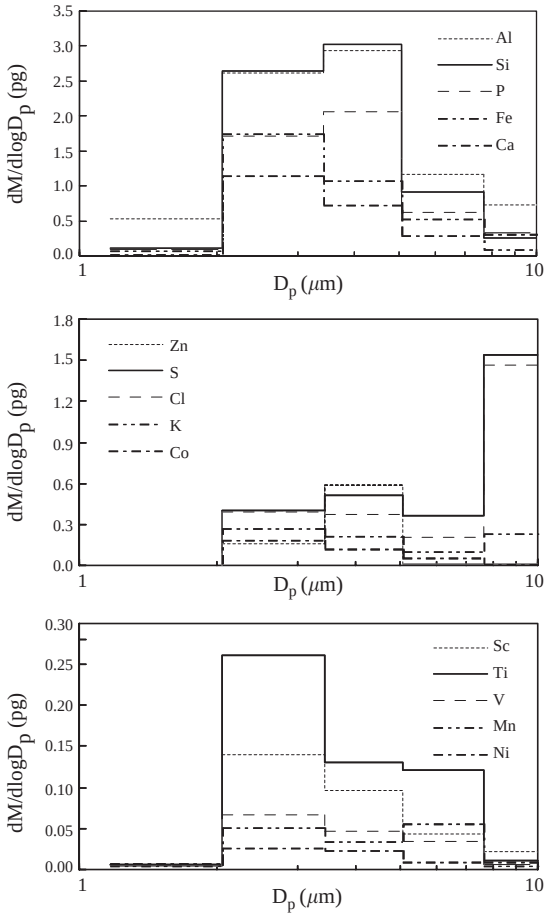

Fig. 6. Average elemental mass of the size-resolved individual Asian dust event particles.

sulfur. The mechanisms for modification of dust particles by sea-salt were most probably collision and coagulation. Consequently, both group 2 and group 3 seem to express the modification of ADS particles with sea-salt and sulfur. These results of our factor analysis can be compared with other studies showing the modification rate of individual ADS particles. Ma et al. (2004) reported the properties of individual ADS particles collected at Kosan (the western tip of Cheju Island), Korea during ACE-Asia. They suggested that 32% of individual ADS particles collected at Kosan were not modified. On the other hand, in our measurement carried out on the west coast of Japan the relatively pure crustal component accounted for 21% of total particle population. In other words, about 79% of individual particles can be classified as particles modified with sea-salt and sulfur. Though there remains more study to fully understand how natural aerosol particles age and how anthropogenic pollutants are incorporated into naturally emitted aerosol particles, the modification reactions of naturally emitted ADS particles are dependent on various conditions. For example, physical condition of the atmosphere such as the path of the prevailing wind and humidity of the air, and gas-phase pollutants like SO_2, NO_x, HCl, and HNO_3. Since our sampling site is located at the western part of Japan, the source materials causing modification of ADS particles are sea-salt and anthropogenic chemical constituents emitted from the inland industrial areas of China, the Korean Peninsula, and marine area. In the previous backward trajectory map the prevailing air parcel developed at 4000 m AGL at 00 UTC on 22 March was arrived at our sampling site across the Korean Peninsula, while an air parcel developed at 3500 m AGL and directly arrived at our sampling site across the southern part of Japan Island. Thus, if 68% of individual Asian dust particles collected at Kosan were already modified over the Chinese continent and the Yellow sea (Ma et al., 2004), our result indicates that the additional aging process in the Korean Peninsula and the southern part of Japan Island is very slight.

4. Conclusions

It is widely recognized that the ADS is a serious and growing environmental problem in East Asia as well as the Pacific Basin. In order to determine the physico-chemical characteristics of individual ADS particles, an intensive field measurement was performed on the west coast of Japan during a dense ADS event in March 2002. From the results, we can draw conclusions as follows:

1. While the number concentration of small particles (ranging from 1.0 to 2.0 μm) was slightly increased during an ADS compared with that of a NADS, the giant particles (larger than 5 μm) marked 124 times higher concentration in an ADS event.
2. From the chemical analysis of individual ADS particles using SPring-8 system, it was possible to reconstruct elemental maps and quantify multiple elemental masses in individual particles.
3. The visualization technique of elemental maps enables us not only to presume the chemical mixing state of individual particles, but also to estimate their source profiles. Furthermore, from this XRF image replayed corresponding to individual particles, we could simply fractionate individual particles.
4. The elemental masses in individual ADS particles showing severe scattering indicate that individual ADS particles collected during our intensive measurement have the complex chemical nature.
5. As might be expected, crustal components especially Si showed remarkably high elemental masses.

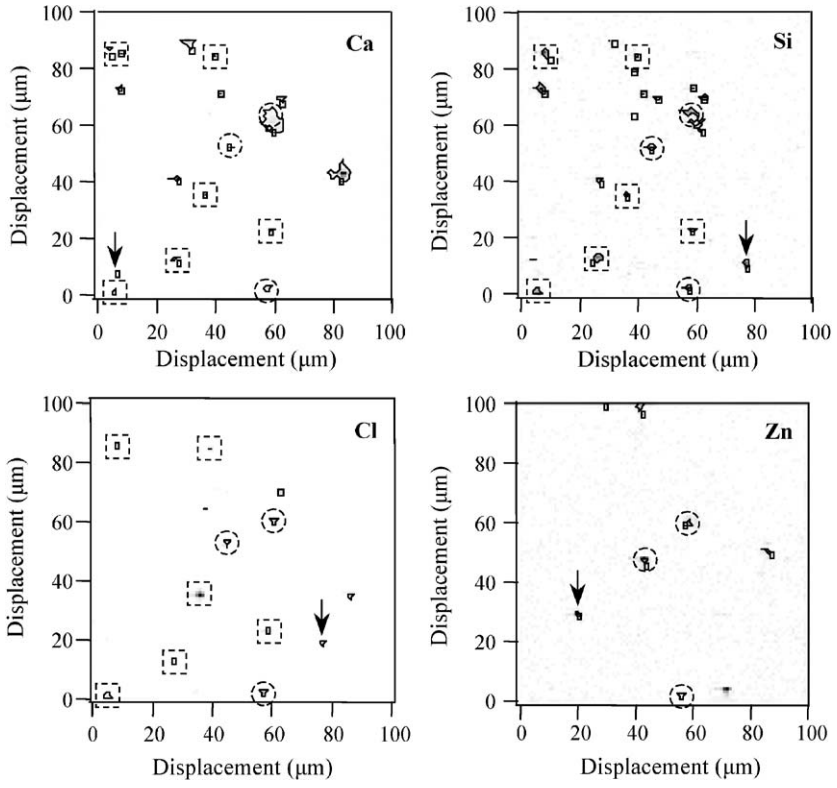

Fig. 7. The XRF images of Ca, Si, Cl, Zn in individual coarse particles (5.07 μm). Ten kilo-electron-volt X-rays were applied for excitation.

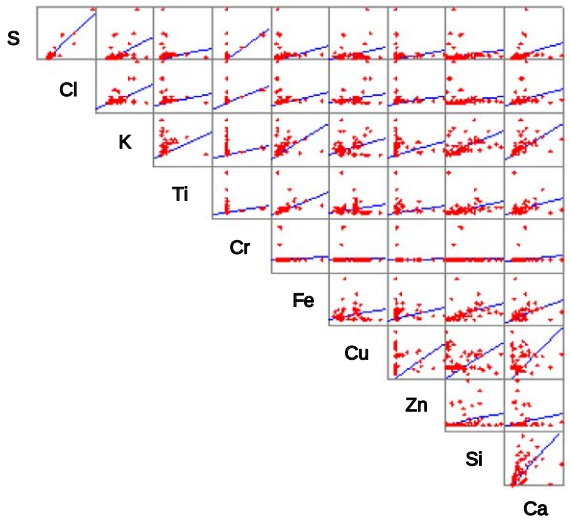

Fig. 8. The interelemental correlation matrix. This squared multiple correlation was obtained from the inverted matrix of interelemental correlations. This correlation matrix was used as the initial data to reduce the number of factors.

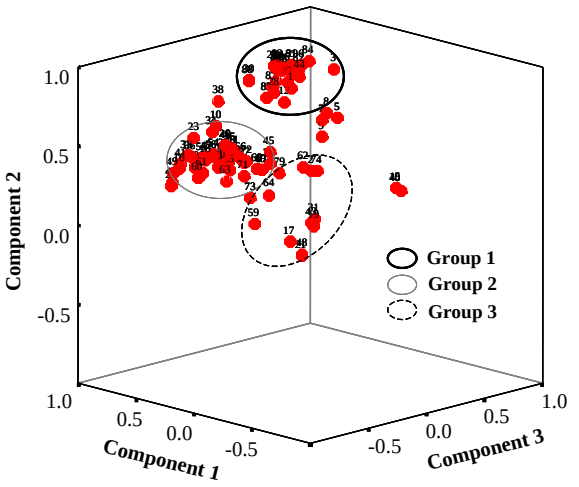

Fig. 9. Components plot in rotated space which is a set of data in 3-D space, i.e. where each point is defined by a x, y and z coordinate. This gives us information about the dimensionality of the data and how the variables are related to each other.

6. From the factor analysis, individual ADS particles were categorized into three groups, i.e. soil components-rich, soil/sulfur-rich, and crustal/marine/sulfur-rich.

Acknowledgements

This study was supported in part by funds from the Grant-in-Aid for Scientific Research on Priority Areas under Grant No. 14048212 and 14048213 from Ministry of Education, Culture, Sports, Science and Technology (MEXT), Japan. Also this study was partly carried out under the aid of the program "Establishment of COE on Sustainable-Energy System". The backward trajectory developed and proffered by the National Oceanic Atmospheric Administration (NOAA) was very helpful to data interpretation. The synchrotron radiation experiments were performed at the SPring-8 with the approval of Japan Synchrotron Radiation Research Institute (JASRI) (Proposal No. 2002B0395-NOS-np, 2002A4029-LM-np). Finally, the authors wish to express thanks to all the members of SPring-8, BL-39XU (at present BL-37XU).

References

Braaten, D.A., Cahill, T.A., 1986. Size and composition Asian dust transported to Hawaii. Atmospheric Environment 20, 1105–1109.

Chun, Y.S., Kim, J.Y., Choi, J.C., Boo, K.O., Oh, S.N., Lee, M.H., 2001. Characteristic number size distribution of aerosol during Asia dust period in Korea. Atmospheric Environment 35, 2715–2721.

Duce, R.A., Unni, C.K., Ray, B.J., Prospere, J.M., Merrill, J.T., 1980. Long-range atmospheric transport of soil dust from Asia to the tropical north Pacific: temporal variability. Science 209, 1522–1524.

Hayakawa, S., Susumu, T., Takagawa, K., Hamamoto, A., Nishida, Y., Suzuki, M., Sato, Y., Hirokawa, T., 2001. Ultra trace characterization using an X-ray microprobe at SPring-8 BL39XU. Analytical Science 17, i115–i117.

Hinz, K.P., Greweling, M., Iflseder, H., Trimborn, A., Spengler, B., 1998. Source identification of single particles by on-line laser mass spectrometry. Journal of Aerosol Science 29, S1253–S1254.

Iwasaka, Y., Yamamoto, M., Imasu, R., Ono, A., 1988. Transport of Asian dust particles (KOSA): importance of weak KOSA events on the geochemical cycle of soil particles. Tellus 40B, 494–503.

Kim, K.H., Choi, G.H., Kang, C.H., Lee, J.H., Kim, J.Y., Youn, Y.H., Lee, S.R., 2003. The chemical composition of fine and coarse particles in relation with the Asian Dust events. Atmospheric Environment 37, 753–765.

Ma, C.J., Tohno, S., Kasahara, M., Hayakawa, S., 2004. Properties of individual Asian dust storm particles collected at Kosan, Korea during ACE-Asia. Atmospheric Environment 38, 1133–1143.

Nishikawa, M., Kanamori, S., 1991. Chemical composition of Kosa aerosol (yellow sand dust) collected in Japan. Analytical Science 7, 1127–1130.

Wang, X., Guanghua, Z., 1996. Some characteristics of the aerosol in Beijing. International Journal of PIXE 6, 361–365.

Zhang, D., Iwasaka, Y., 1998. Morphology and chemical composition of individual dust particles collected over Wakasa bay, Japan. Journal of Aerosol Science 29, S217–S218.

Zhang, J., Wu, Y., Liu, C.L., Shen, Z.B., Yu, Z.G., Zhang, Y., 2001. Aerosol characters from the desert region of Northwest China and the Yellow sea in spring and summer: observations at Minqin, Qingdao, and Qinliyan in 1995–1996. Atmospheric Environment 35, 5007–5018.